Journal of Manufacturing Processes 124 (2024) 590–603

Contents lists available at ScienceDirect

Journal of Manufacturing Processes

journal homepage: www.elsevier.com/locate/manpro

Optimization of metal transfer in rutile flux-cored arc welding through controlled CO_2 concentration in argon–CO_2 shielding gas

Ngoc Quang Trinh [a], Khoi Dang Le [b], Shinichi Tashiro [b,*], Tetsuo Suga [b], Shuji Sasakura [c], Kazuhiro Fukuda [c], Anthony B. Murphy [d], Hanh Van Bui [a,*], Manabu Tanaka [b]

[a] School of Mechanical Engineering, Hanoi University of Science and Technology, Vietnam
[b] Joining and Welding Research Institute, Osaka University, Japan
[c] Kobe Steel, Ltd., Japan
[d] CSIRO Manufacturing, Australia

ARTICLE INFO

Keywords:
Flux-cored arc welding
Rutile flux-cored wire
Shielding gas
Metal vapor
Arc plasma
Flux column
Metal transfer

ABSTRACT

In this study, we analyzed the impact of carbon dioxide concentration in argon–carbon dioxide shielding gas on droplet transfer characteristics in rutile flux-cored arc welding, employing titanium oxide as a primary wire flux component. The welding process was carried out at a welding current of 190, 220, 250, 280, and 310 A under an argon–CO_2 shielding gas mixture with six levels of CO_2 concentration of 0, 5 %, 10 %, 15 %, 20 %, and 25 % for a parametric study. Unlike the conventional solid wire welding trend, where the droplet transfer frequency decreases with the increase in carbon dioxide concentration, an increase in metal transfer frequency was observed with the increase in CO_2 concentration from approximately 5 % to 20 %. The concentration reaching the maximum frequency was 20 % at 190 A, which decreased as the welding current increased, reaching 5 % at 310 A. Droplet initiation at the lower sheath end is succeeded by a gradual downward movement along the flux column's side after a few milliseconds. Upon reaching the lower end, the droplet forms a neck and undergoes separation. Thus, the length of the flux column directly impacts the duration of one droplet transfer cycle. The length was decreased by arc constriction when increasing CO_2 concentration appropriately to concentrate beneath the flux column or by increasing the welding current to raise the arc temperature, which contributed to melting and shortening the flux column.

1. Introduction

Flux-cored wire arc welding (FCAW) is an enhanced welding technique derived from gas metal arc welding (GMAW), wherein a traditional solid wire is substituted with a tubular wire containing a welding powder encased within a metal wire sheath. The distinctive configuration of this wire imparts numerous advantages to the welding process, particularly for augmentation of the deposition rate and enhancement in the flexibility of the filler material composition [1]. The adaptable flux composition inherent in FCAW enables its execution with an external shielding gas in conventional welding scenarios or broadens its application to welding in diverse environments, including field or underwater settings, using a self-shielding wire [2,3].

The FCAW with a shielding gas was generally classified into subgroups as rutile flux-cored, metal flux-cored, and basic flux-cored based on the flux formulation. In the rutile flux-cored wire, the main composition of the flux is rutile (TiO_2), which provides a good slag characteristic and arc stability [4]. The metal flux-cored wire has primarily iron and alloy powder in the flux. This wire provides a high deposition rate and good arc stability when a mixture of argon–carbon dioxide shielding gas is used [5]. On the other hand, the basic flux-cored wire is preferred when control of the amount of diffusion hydrogen is considered, owing to fluorides, such as CaF_2 or KF, included in the flux powder [6,7]. In addition, the addition of some alloys can improve the hardness of the surface. The flux-cored wire can be designed for hardfacing and cladding purposes [8,9].

As for other welding processes using a consumable electrode, the molten metal transfer process in FCAW strongly influences welding stability and performance [10]. The metal transfer process was investigated intensively for the GMAW process but was rarely mentioned for the FCAW process. The metal transfer regime in FCAW was considered to be more complicated than GMAW under the welding parameters due

* Corresponding authors.
E-mail addresses: tashiro.shinichi.jwri@osaka-u.ac.jp (S. Tashiro), hanh.buivan@hust.edu.vn (H.V. Bui).

https://doi.org/10.1016/j.jmapro.2024.06.047
Received 31 March 2024; Received in revised form 30 May 2024; Accepted 17 June 2024
Available online 21 June 2024

Table 1
Chemical composition (mass%) of the investigated wire.

Wire	C	Si	Mn	SiO_2	TiO_2
Flux-cored wire	0.05	0.67	2.53	0.63	5.62

to the wire characteristics. For example, the effect of the wire structure was investigated by Matsuda et al., who reported that the droplet diameter of a folded-shaped wire is smaller than that of a hollow-shaped wire [11]. In addition, when the flux ratio in the wire was increased, the fume emission rate decreased [12], while the metal transfer frequency was increased with the welding current [13].

Regarding the effect of the flux composition, the main flux formulation determines the difference in metal transfer behavior. Starling and

Table 2
Welding conditions.

Welding current level	CO_2 concentration in the gas mixture (%)	Setting current (A)	Setting voltage (V)	Output current (A)	Output voltage (V)	Wire feeding speed (m/min)
	0 %	245	22.5	190	24.0	7.6
	5 %	247	24.5	191	25.8	7.7
	10 %	247	26.0	190	27.1	7.7
	15 %	247	27.5	189	28.2	7.7
	20 %	247	29.3	194	29.8	7.7
190 A	25 %	250	30.5	195	31.4	7.9
	0 %	265	24.0	217	25.7	8.8
	5 %	268	25.5	219	27.1	9.0
220 A	10 %	270	27.0	219	28.5	9.2
	15 %	270	28.5	223	29.8	9.2
	20 %	270	30.5	225	31.6	9.2
	25 %	270	32.0	221	33.0	9.2
	0 %	290	22.5	247	26.8	10.5
	5 %	290	27.0	252	28.1	10.5
250 A	10 %	290	28.5	251	29.6	10.5
	15 %	290	30.5	250	31.6	10.5
	20 %	295	32.0	251	22.1	10.8
	25 %	295	33.5	253	34.5	10.8
	0 %	315	27.0	277	28.1	12.1
	5 %	320	28.5	282	29.5	12.5
280 A	10 %	320	30.5	279	316	12.5
	15 %	320	32.0	279	33.1	12.5
	20 %	325	33.5	283	34.6	12.8
	25 %	325	25.0	282	36.1	12.8
	0 %	340	28.5	309	29.5	13.8
	5 %	350	30.5	310	31.7	14.5
310 A	10 %	350	32.0	309	33.2	14.5
	15 %	350	33.5	306	34.8	14.5
	20 %	350	35.0	309	36.2	14.5
	25 %	355	36.5	311	37.7	14.8

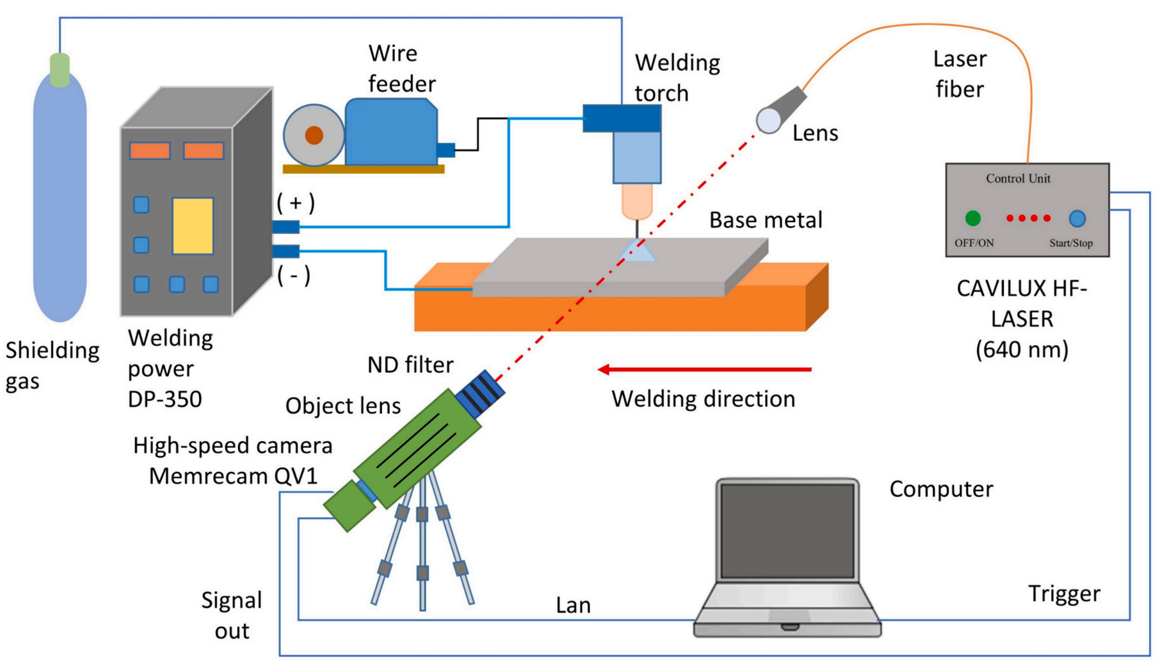

Fig. 1. Schematic of the experimental setup.

Table 3
Visualization conditions.

Parameter	Value
Camera	Nac, Memrecam Q1v
Frame rate	4000 fps
Exposure time	20 μs
Lens	AI AF Micro-Nikkor 200 mm f/4D IF-ED
Aperture	*f*/5.6
Neutral filter	5 × ND-8
Laser wavelength	640 nm

Modenesi [14] showed that the shielding gas composition influenced the metal transfer behavior in all three types of flux-cored wires, in which the metal-cored wire exhibited a similar transfer regime to that of a solid wire. In contrast, the basic flux-cored wire exhibited the most unstable arc among these wires. On the other hand, the addition of alkaline elements to the flux formulation can significantly improve the arc and metal transfer stability. Valensi et al. [15] reported that a cored wire with high alkaline and silicon contents in the flux can maintain a stable spray transfer with a mixture of shielding gas with a CO_2 content of up to 60 % at a welding current of 330 A. Trinh et al. also investigated the effect of sodium on the metal transfer for a metal-cored wire [16]. The metal transfer frequency increased with the sodium concentration in the

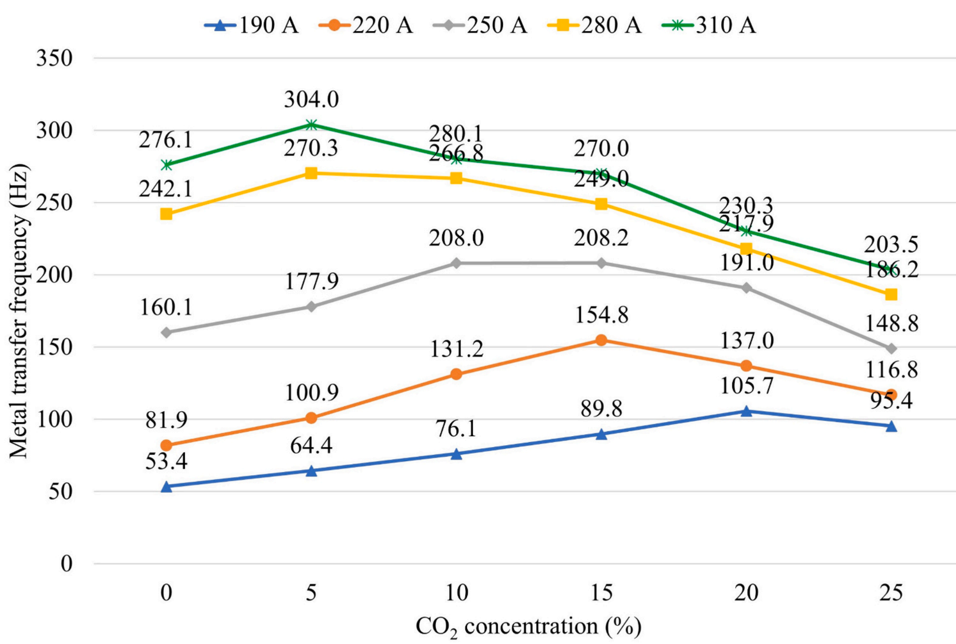

Fig. 2. Metal transfer frequency as a function of the CO_2 concentration.

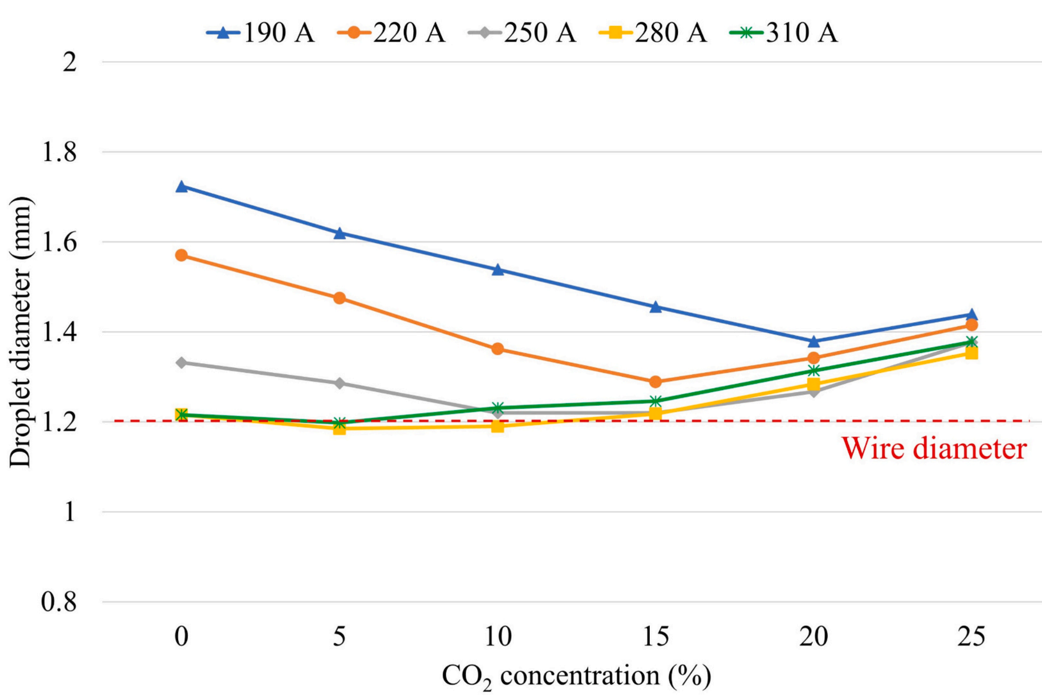

Fig. 3. Calculated droplet diameter as a function of the CO_2 concentration.

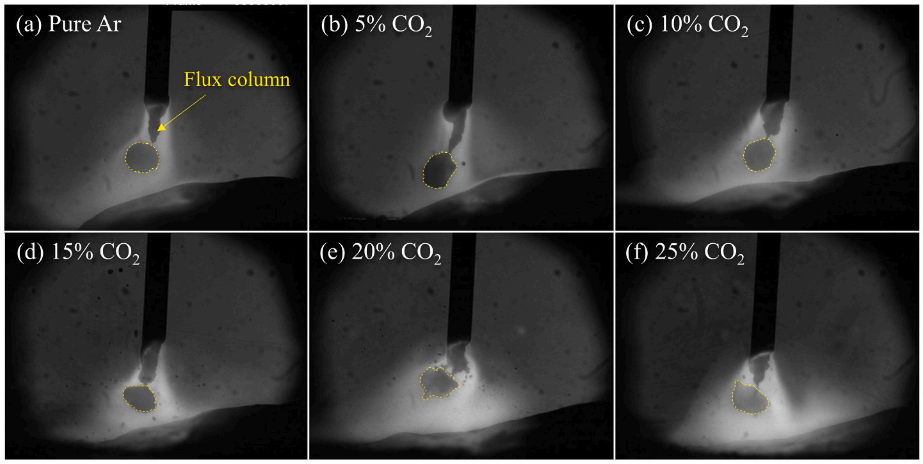

Fig. 4. Typical images of metal transfer at a welding current of 190 A.

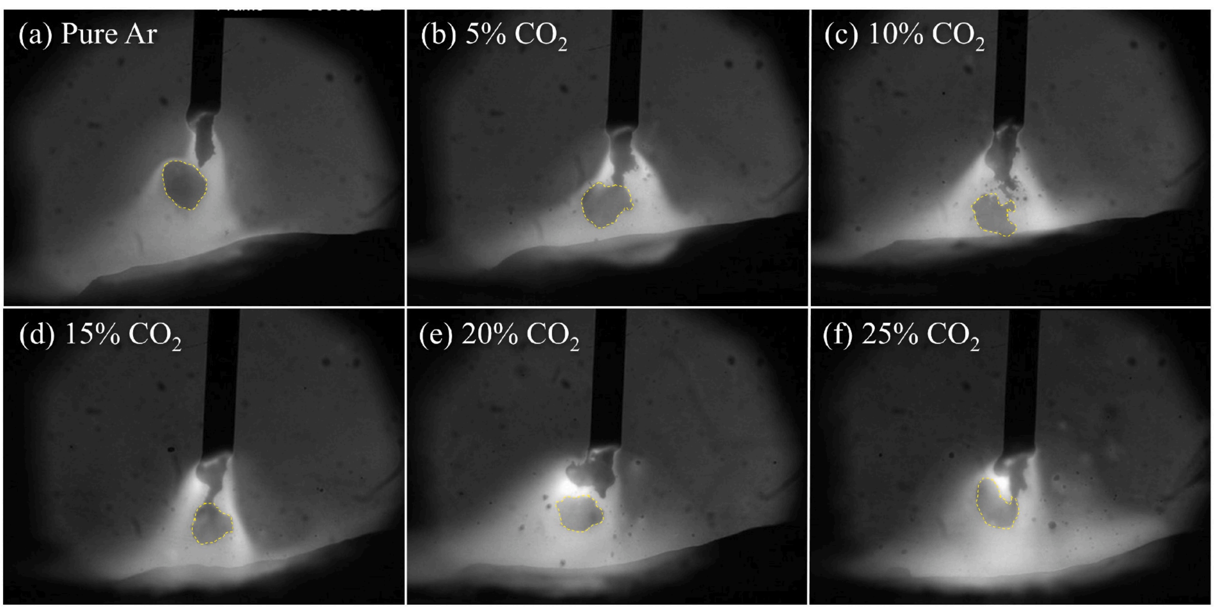

Fig. 5. Typical images of metal transfer at a welding current of 250 A.

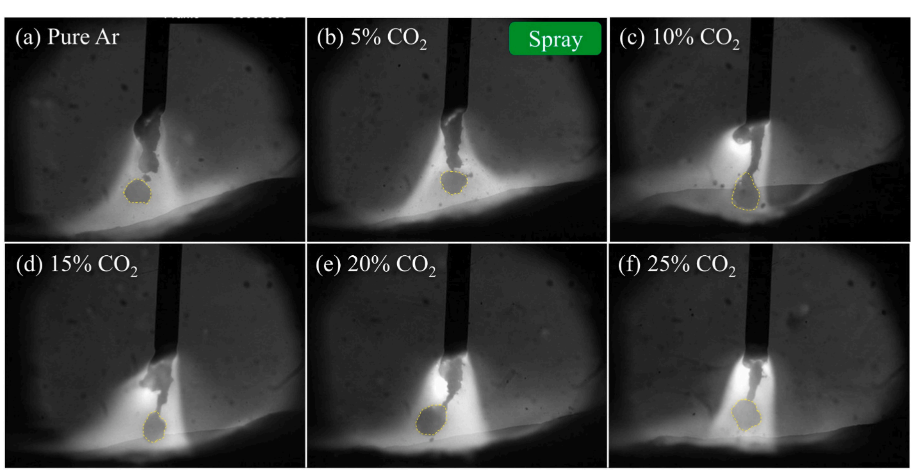

Fig. 6. Typical images of metal transfer at a welding current of 310 A.

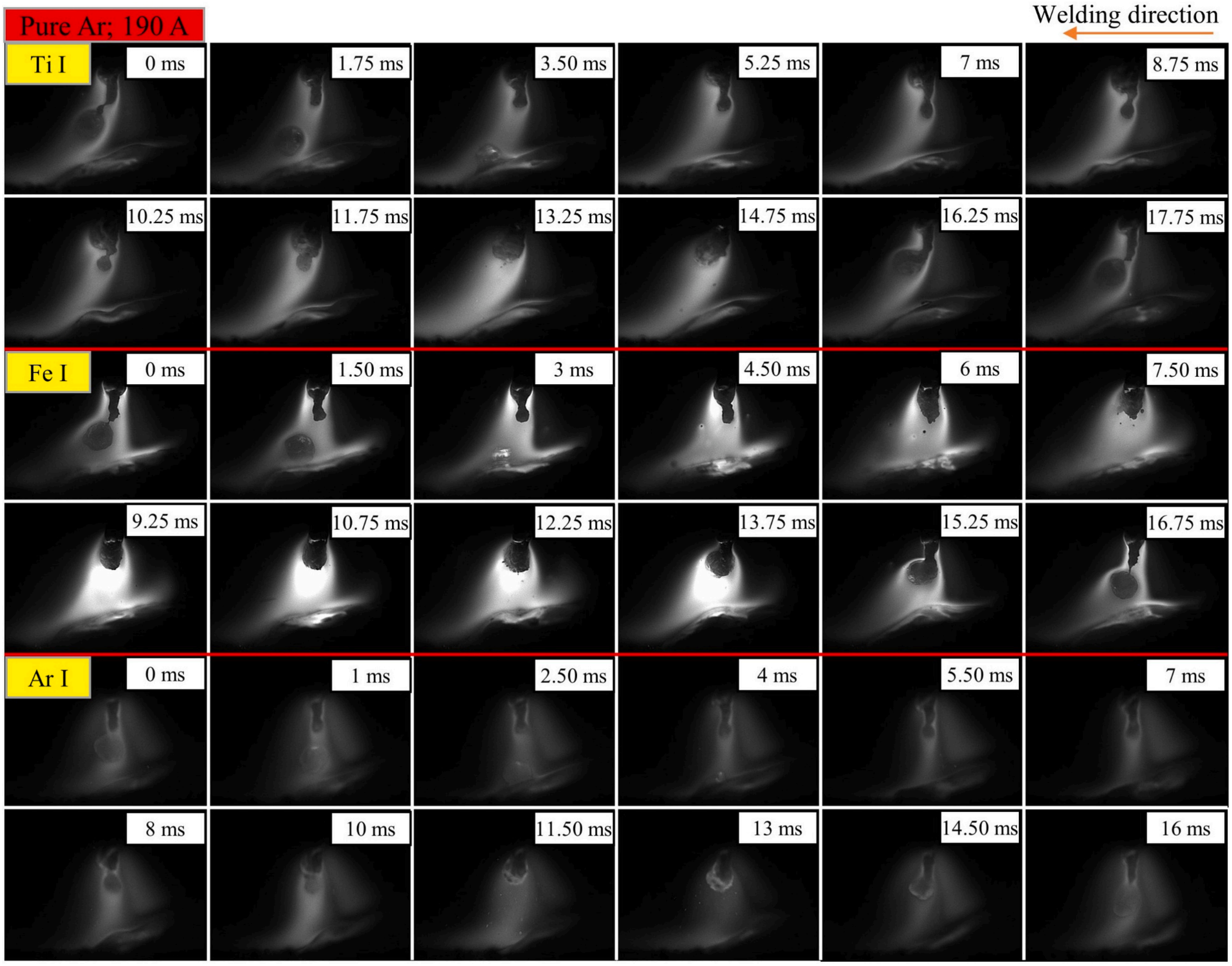

Fig. 7. Arc behaviors observed by the bandpass filters at 190 A using pure argon gas.

flux. Furthermore, the effect of sodium in a metal-cored wire was implied to be more dominant than that of the wire structure, according to Bui et al. [17]. They observed that a metal-cored wire with sodium could extend the transition current over 310 A in a pure argon shielding gas.

Regarding the welding parameters, the welding current and shielding gas were considered dominant factors affecting the metal transfer behavior [18,19]. For example, Wang et al. evaluated the metal transfer of a flux-cored wire through an electrical arc signal, droplet diameter, and high-speed imaging measurement [20]. They reported that several different metal transfer modes could have coexisted simultaneously. The effect of the shielding gas on the metal transfer of a metal-cored wire was investigated by Trinh et al. [21]. They observed that the gas and metal vapor plasmas were closely attached to the wire tip, and that the unmelted flux at the wire tip did not facilitate the streaming transfer as in a solid wire.

Notably, even the research trend on the flux-cored wire was focused on the application rather than the physical phenomena during the process [22]. As mentioned, the arc and metal transfer during the FCAW were considered to be complex. Thus, the welding performances under wide ranges of welding current and shielding gas have not been well elucidated.

In this study, we investigated the welding process with a commercial flux-cored wire under six types of shielding gas, including pure argon and argon–CO_2 shielding gas mixtures with CO_2 percentages of 5 %, 10 %, 15 %, 20 %, and 25 %. These six shielding gas mixtures were investigated for a parametric study at five welding current levels of 190, 220, 250, 280, and 310 A. The metal transfer behavior was evaluated through a visualization by a high-speed camera system. In addition, plasma diagnosis by observation of the plasma spectra was also implemented to clarify the mechanism of the influences of CO_2 concentrations on the metal transfer behavior of the rutile flux-cored wire.

2. Experimental method

2.1. Welding parameters

We implemented a series of experiments to clarify the metal transfer behavior and arc phenomenon in the FCAW process on a mild steel plate (JIS-SS400) as a base material. The commercial rutile flux-cored wire corresponds to an American Welding Society (AWS) classification of A5.20 E70T-1C, with the main content of the flux being TiO_2. The electrode diameter was 1.2 mm. The chemical composition of the wire is shown in Table 1.

The welding is carried out in a direct-current electrode positive setting using a welding source power (DP-350, OTC-Daihen) with six types of mixture shielding gas of argon–CO_2 with CO_2 concentrations of 0, 5 %, 10 %, 15 %, 20 %, and 25 %. The gas flow rate was maintained at 20 L/min. The welding current was applied at five levels of 190, 220, 250, 280, and 310 A to assess the arc characteristics and metal transfer behavior. The welding voltage was adjusted from 27 to 36.5 V during the experimental procedure to ensure a constant arc length. The distance from the contact tube to the surface of the workpiece was 20 mm. The welding velocity was 5 mm/s. The welding current, welding voltage,

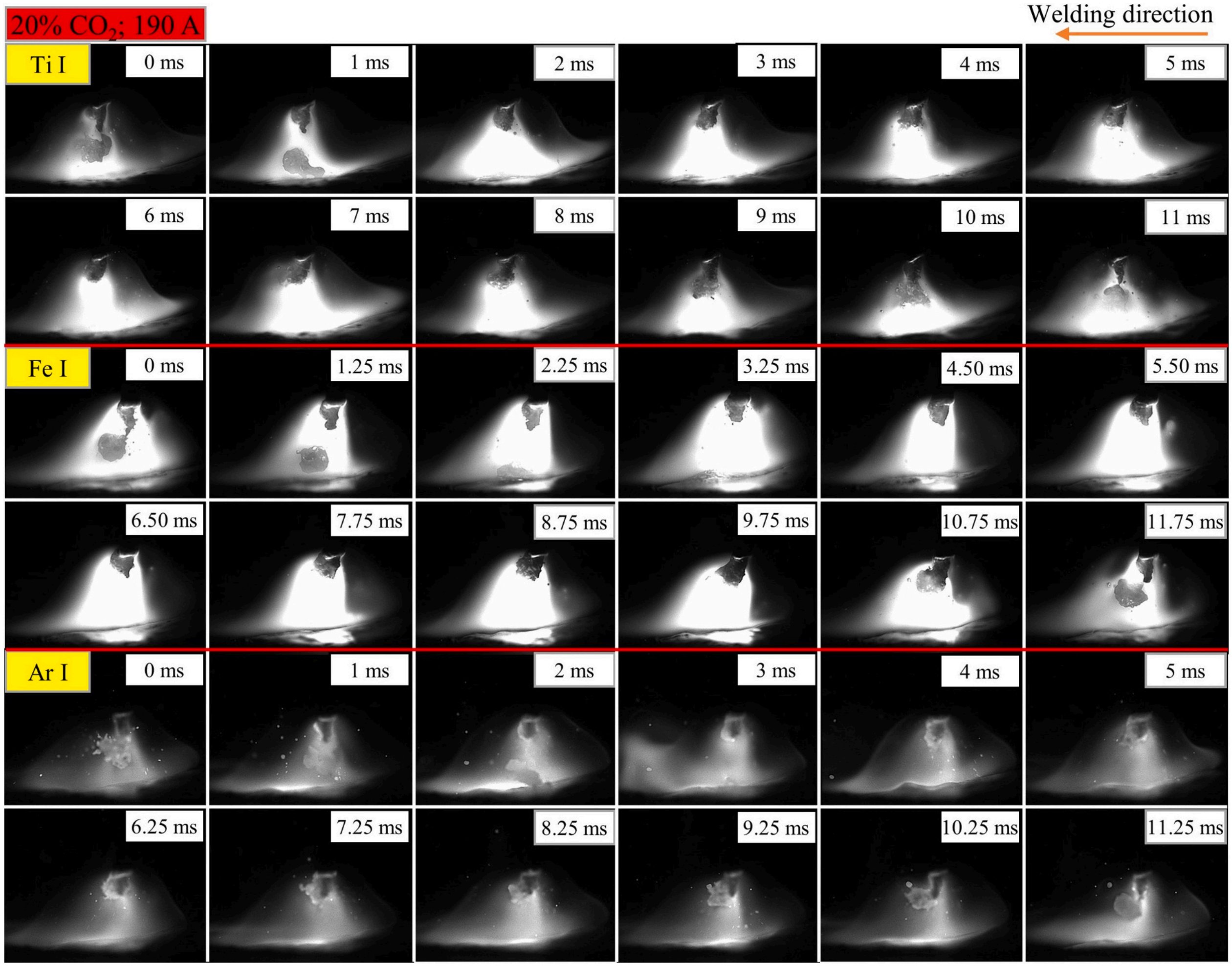

Fig. 8. Arc behaviors observed by bandpass filters at 190 A using the Ar + 20 % CO_2 gas.

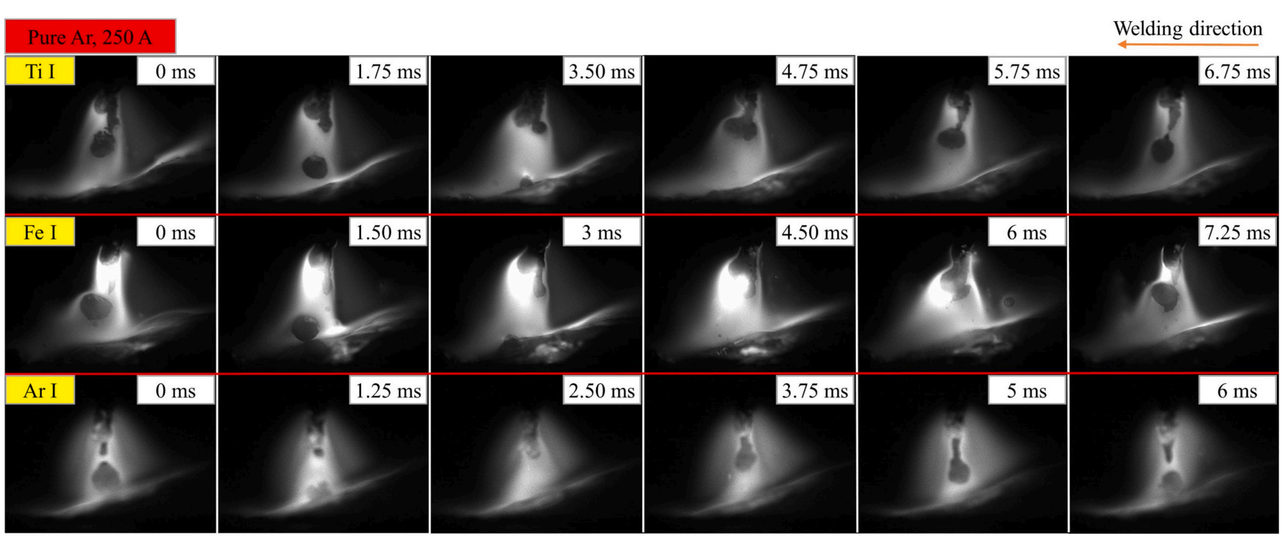

Fig. 9. Arc behaviors observed by bandpass filters at 250 A using pure Ar gas.

and wire feeding speed are listed in Table 2.

2.2. Visualization conditions

We combined a high-speed camera (Memrecam Q1v, Nac Image Technology, Minato, Japan) with a laser illumination system (Cavilux HF, Cavitar, Tampere, Finland) to observe the metal transfer and arc phenomenon based on the shadowgraph technique. The welding arc is aligned in the middle of the laser and camera lenses, as depicted in Fig. 1. The laser system was used in the high-frequency mode, producing

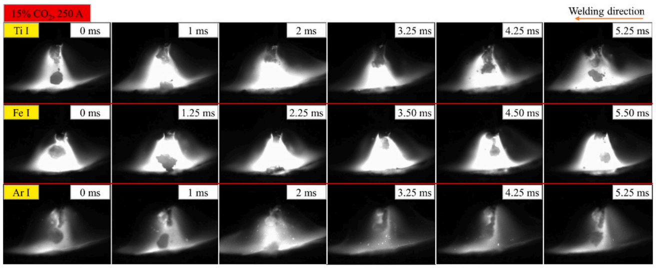

Fig. 10. Arc behaviors observed by bandpass filters at 250 A using the Ar + 15 % CO_2 gas.

a pulse laser light with a wavelength of 640 nm at 4444 Hz for 10 s. The frequency of the laser light was higher than the camera frame rate of 4000 fps at an exposure time of 20 μs, which prevented the camera imaging from being disturbed. Other observation parameters are presented in Table 3.

Some characteristics of the arc plasma in the welding process were reflected in the plasma distribution of the electrically charged particles in the plasma. In this study, spectral visualization was conducted to diagnose the arc behavior further to investigate the plasma distribution for significant elements. Three bandpass filters were equipped on the camera to individually observe the plasmas of titanium, iron, and argon species. The filters were denoted as Ti I, Fe I, and Ar I, with center wavelengths of 568.0, 540.0, and 695.5 nm, respectively. All filters were designed with a full width at half maximum of 10.0 nm.

3. Results and discussion

3.1. Droplet transfer regime

Fig. 2 depicts metal transfer frequencies of the flux-cored wire as a function of the CO_2 concentration with the investigated welding conditions. The measurement was achieved after counting ten times for an acquisition of 250 ms. The frequency increased when the welding current increased. Under the effect of the CO_2 percentage in the range of 0 to 25 %, the frequency at each current level exhibited a peak value. For example, the frequency at 190 A increased from 53.4 to 105.7 Hz when %CO_2 increased from 0 to 20 %, and then decreased to 95.4 Hz at 25 % CO_2 in the shielding gas. When the current was 220 A, the frequency increased from 81.9 to 154.8 Hz and decreased to 116.8 Hz at CO_2 concentrations of 0, 15 %, and 25 %, respectively. At a welding current of 250 A, the frequency increased from 160.1 Hz to approximately 208.2 Hz and decreased to 148.8 Hz when the CO_2 content was 0, 15 %, and 25 %, respectively. At that level, the frequencies at CO_2 contents of 10 % and 15 % were almost equal. When the welding current was increased to 280 and 310 A, the maximum frequency was 270.3 and 304.0 Hz, respectively, at a CO_2 content of 5 %. The effect of the CO_2 concentration on the transfer frequency had a similar tendency for all welding currents in which the frequency peaked at a critical CO_2

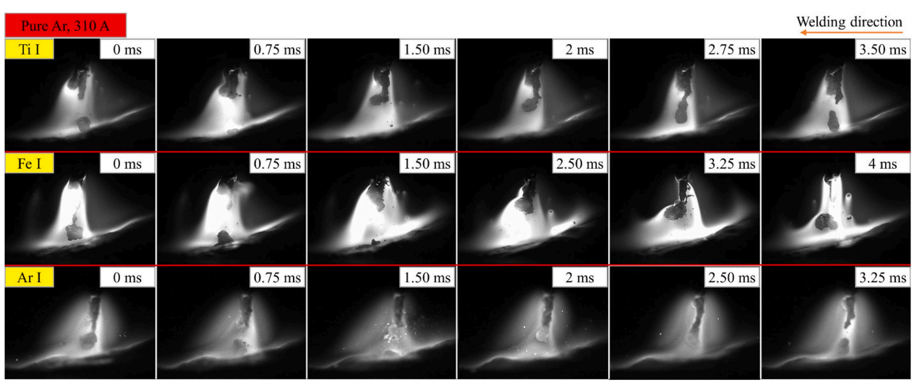

Fig. 11. Arc behaviors observed by the bandpass filters at 310 A using pure argon gas.

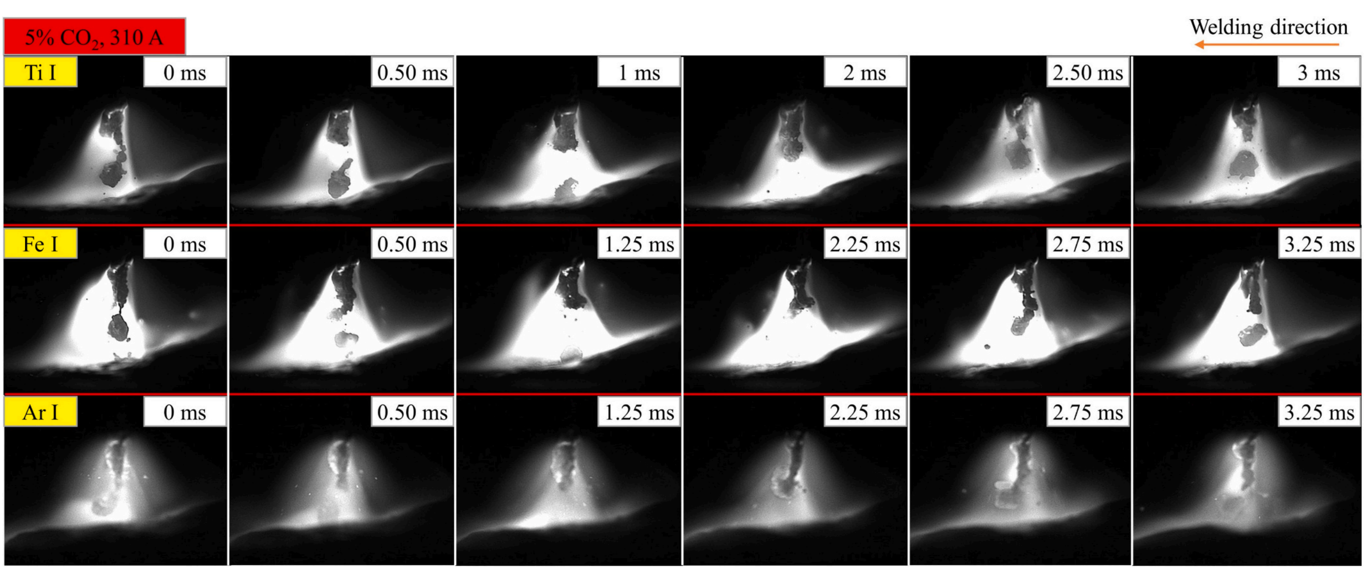

Fig. 12. Arc behaviors observed by the bandpass filters at 310 A using the Ar + 5 % CO_2 gas.

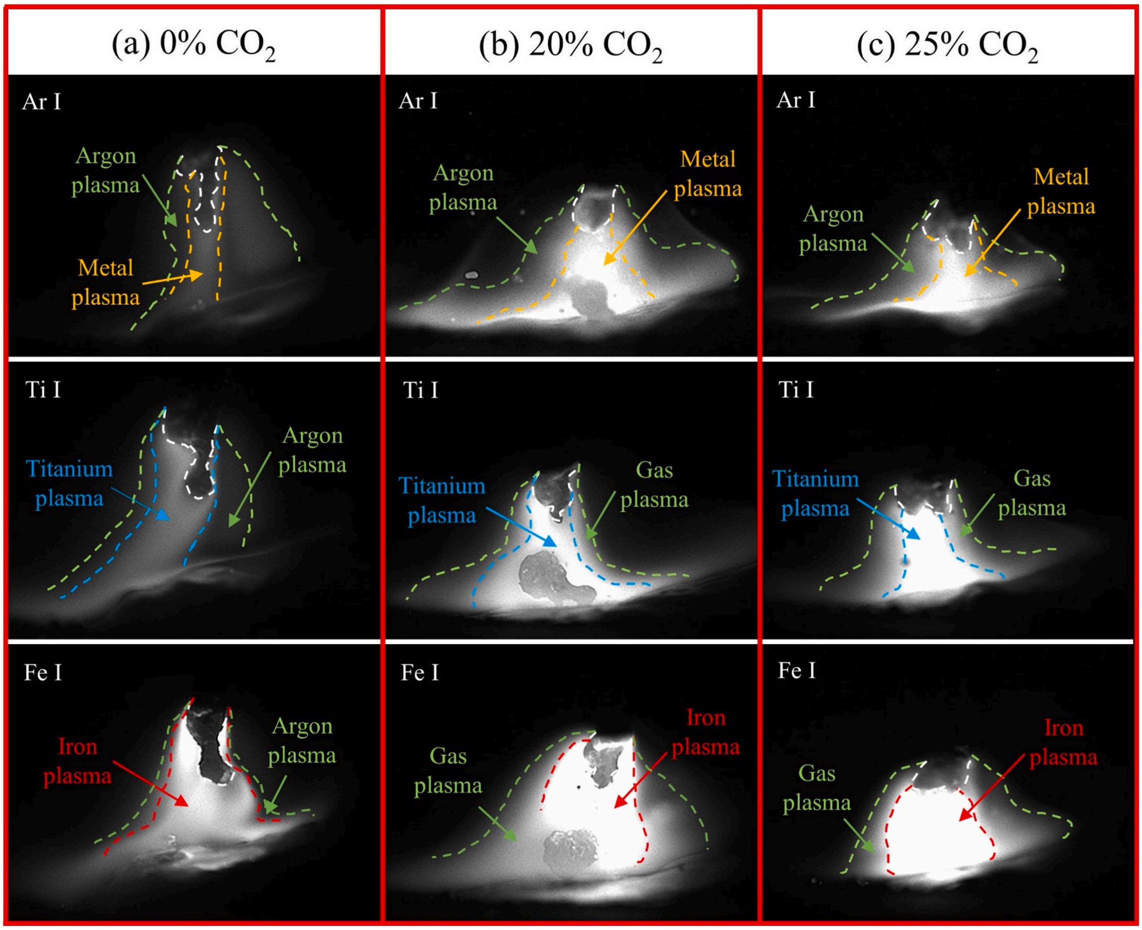

Fig. 13. Arc plasma distributions at 190 A obtained using CO_2 concentrations of 0 % (a), 20 % (b), and 25 % (c) in the shielding gas.

concentration. However, the critical concentration was decreased when the welding current was increased.

Fig. 3 shows the droplet diameter obtained by the metal transfer frequency. During the welding process, a droplet was assumed to be a homogeneous sphere, and its diameter was calculated to be similar to that in a previous study [21]. The result was also compared to the wire diameter of 1.2 mm to clarify the metal transfer regime. The metal transfer regime at 280 A at 5 % and 10 % and that at 310 A at 5 % of CO_2 showed the spray transfer, in which the droplet diameter was smaller than the wire diameter. Even though the frequency at the welding current of 310 A was higher than those at 280 and 250 A under some conditions, the droplet diameter exhibited a larger value. It can be considered that the high wire feed speed at 310 A increased the total volume of a molten droplet.

Fig. 4 shows typical images of droplet transfer at a welding current of 190 A. As observed in Fig. 3, the droplet was transferred in the globular mode. In Fig. 4(a), under the pure argon gas, a flux column is maintained at the tip of the electrode. The arc position was thought to be attached to the interface region of the solid and liquid of the metal sheath. The arc had a narrow and conical shape. The flux column was also observed. Its length was reduced when the CO_2 concentration was increased. As shown in Fig. 4(f), the arc plasma was broadened, and the brightness area was changed to a bell shape when the CO_2 content was 25 %.

The metal transfer behaviors at 190, 250, and 310 A are presented in this manuscript as corresponding to the lowest, middle, and highest welding current levels, respectively. Fig. 5 shows the typical images of droplet transfer at 250 A. The molten droplets at 10 % and 15 % CO_2 are smaller than those under the other conditions, as depicted in Fig. 5(c) and Fig. 5(d). The metal transfer images at 310 A are shown in Fig. 6. In Fig. 6(b), the metal transfer regime is classified as spray transfer, according to Fig. 3. Similar to those at the welding currents of 190 and 250 A, there is an unmelted flux column at the tip of the wire at 310 A.

3.2. Arc characteristics

As delineated in the preceding section, the metal transfer behavior reveals a frequency peak at a critical CO_2 concentration. This concentration exhibited a decrease with the increase in the welding current. Such a phenomenon has not yet been reported for rutile flux-cored welding. In this investigation, spectroscopy experiments were conducted to analyze arc characteristics and comprehend this observed phenomenon. The observation was applied at three welding currents of 190, 250, and 310 A with the shielding gas without CO_2, at the critical CO_2 concentration (20 %, 15 %, and 5 % at 190, 250, and 310 A, respectively), and at a CO_2 concentration of 25 % to highlight the effect of shielding gas function.

Fig. 7 presents time-sequenced images of one cycle for a droplet transfer observed by three bandpass filters, Ti I, Fe I, and Ar I, using pure argon gas at a welding current of 190 A. The figure indicates that the time for one droplet transfer is approximately 16 to 17.75 ms. Under the same observed conditions, the image of the arc plasma obtained by the Fe I filter was brighter than those obtained by the Ti I and Ar I filters, which implies that the iron plasma had higher radiation than the titanium and argon plasmas. Fig. 8 shows a droplet transfer with 20 % CO_2 during the welding, where the frequency peaked at 190 A. The droplet formation and detachment time is approximately 11 to 11.75 ms. The arc intensity under this condition is higher than that in the pure argon gas.

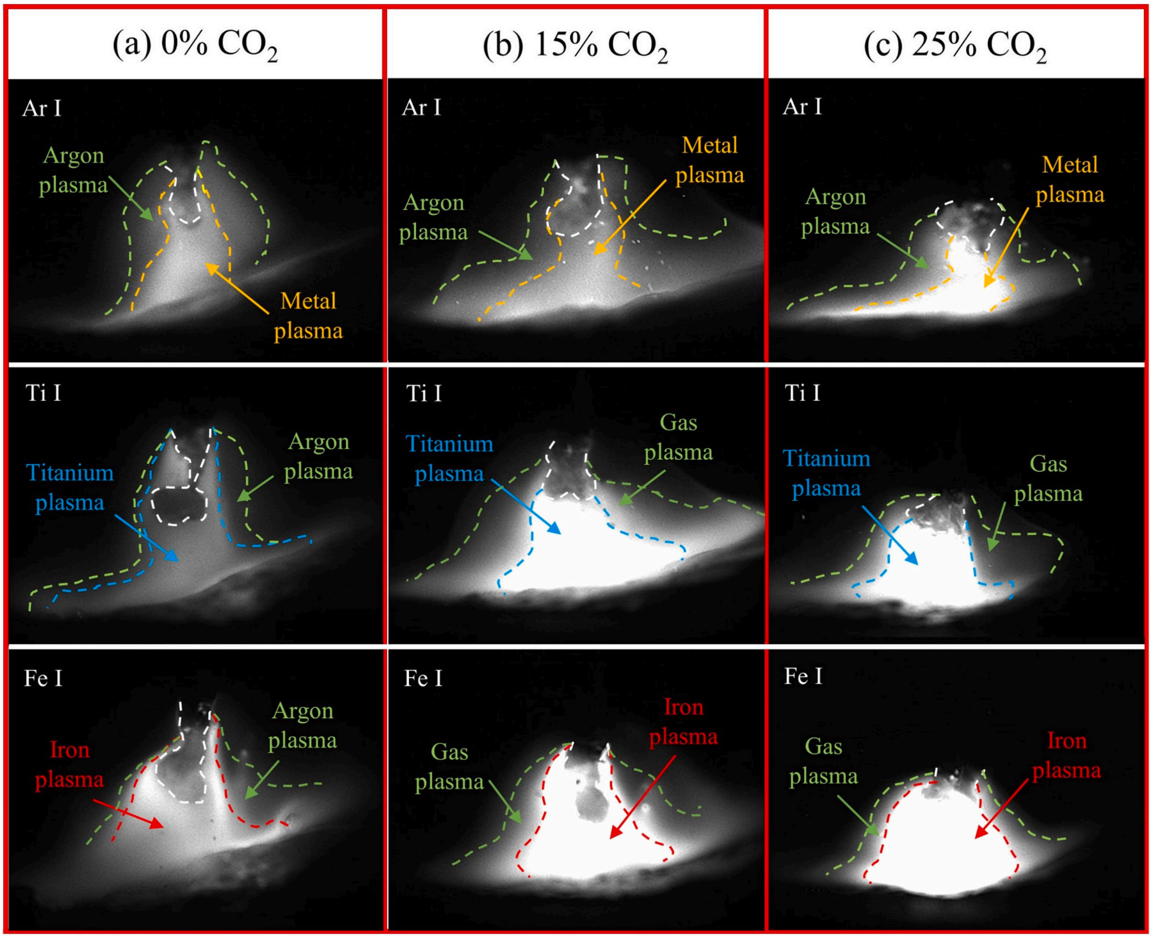

Fig. 14. Arc plasma distributions at 250 A at CO_2 concentrations of 0 % (a), 15 % (b), and 25 % (c) in the shielding gas.

Fig. 9 and Fig. 10 show the metal transfers of pure argon and Ar + 15 % CO_2 shielding gas at a welding current of 250 A, respectively. The time necessary for a droplet transfer was reduced from approximately 6.75 ms to 5.25 ms. In Fig. 9, the image observed by the Fe I filter shows a high-intensity area that completely covers a molten droplet, as shown at the moments of 3, 4.5, and 6 ms. The results at 15 % CO_2 in the shielding gas in Fig. 10 show a higher arc plasma intensity than that of the pure argon in Fig. 9 in each bandpass filter image, owing to the higher CO_2 concentration in the shielding gas. In GMAW, the arc becomes constricted when carbon dioxide is added to the argon shielding gas due to the high specific heat of the additional gas. CO_2 is a molecular gas. Its plasma exhibits a higher electrical conductivity than those of noble gases such as argon. The molecular nature of CO_2 and its specific ionization characteristics contribute to the increased conductivity, which leads to a more focused and constricted arc [23,24].

In addition, Fig. 11 and Fig. 12 show the metal transfer behaviors observed by the bandpass filters at 310 A for pure argon and Ar + 5 % CO_2 shielding gas, respectively. The arc behaviors were consistent with those of the two lower welding currents of 190 and 250 A. The unmelted flux column was relatively long at the welding current of 310 A, particularly when the arc behavior in Fig. 12 is compared to that in Fig. 10. The time for a droplet transfer in pure argon gas was approximately 3.5 ms, which decreased to approximately 3.0 ms when 5 % CO_2 was included in the shielding gas.

Fig. 13 compares the arc plasma distributions at a welding current of 190 A for CO_2 concentrations of 0, 20 %, and 25 % by displaying argon, titanium, and iron plasma concentrations. The term metal plasma was used in the figure to indicate the combined distribution of titanium and iron plasmas when the Ar I filter was applied. In addition, when Ti I and Fe I filters were applied for a shielding gas including CO_2, the term gas plasma was denoted to indicate the plasma distributions of gas species, including argon, carbon, and oxygen. The length of the plasma distribution decreased with the increase in the content of CO_2. As mentioned, the arc constriction is due to the high specific heat when CO_2 is included, which leads to higher metal vapor evaporation and arc radiation than those with pure argon gas. The titanium vapor plasma exhibits significant emissions in Fig. 13(b) and Fig. 13(c) compared to Fig. 13(a), which indicates higher titanium evaporations at 20 % and 25 % CO_2. In Fig. 13 (c), the titanium vapor concentrated in a column at the arc center under the flux column, which was narrower than the bell-shaped distribution of the iron plasma.

Fig. 14 compares the arc plasma distributions at 250 A at 0, 15 %, and 25 % CO_2 in the shielding gas. In addition, at 310 A, the peak frequency was observed at a CO_2 concentration of 5 %. The distributions of argon, titanium, and iron plasmas at this welding current are illustrated in Fig. 15. The distributions at these two welding currents align with that observed at 190 A in Fig. 13. In Fig. 15, the flux column at 310 A is prolonged compared to those under the other conditions, potentially influenced by Joule heating effects, as elaborated later.

3.3. Droplet transfer mechanism in FCAW

Fig. 16 depicts images and schematics of the formation and detachment of a droplet in FCAW at a welding current of 190 A with the pure argon shielding gas. It was inferred that a droplet primarily originated from the molten metal sheath with a contribution from a portion of the molten flux. In Fig. 16(a), a droplet was formed at the end of the metal sheath at an early stage, growing on one side of the flux column. In

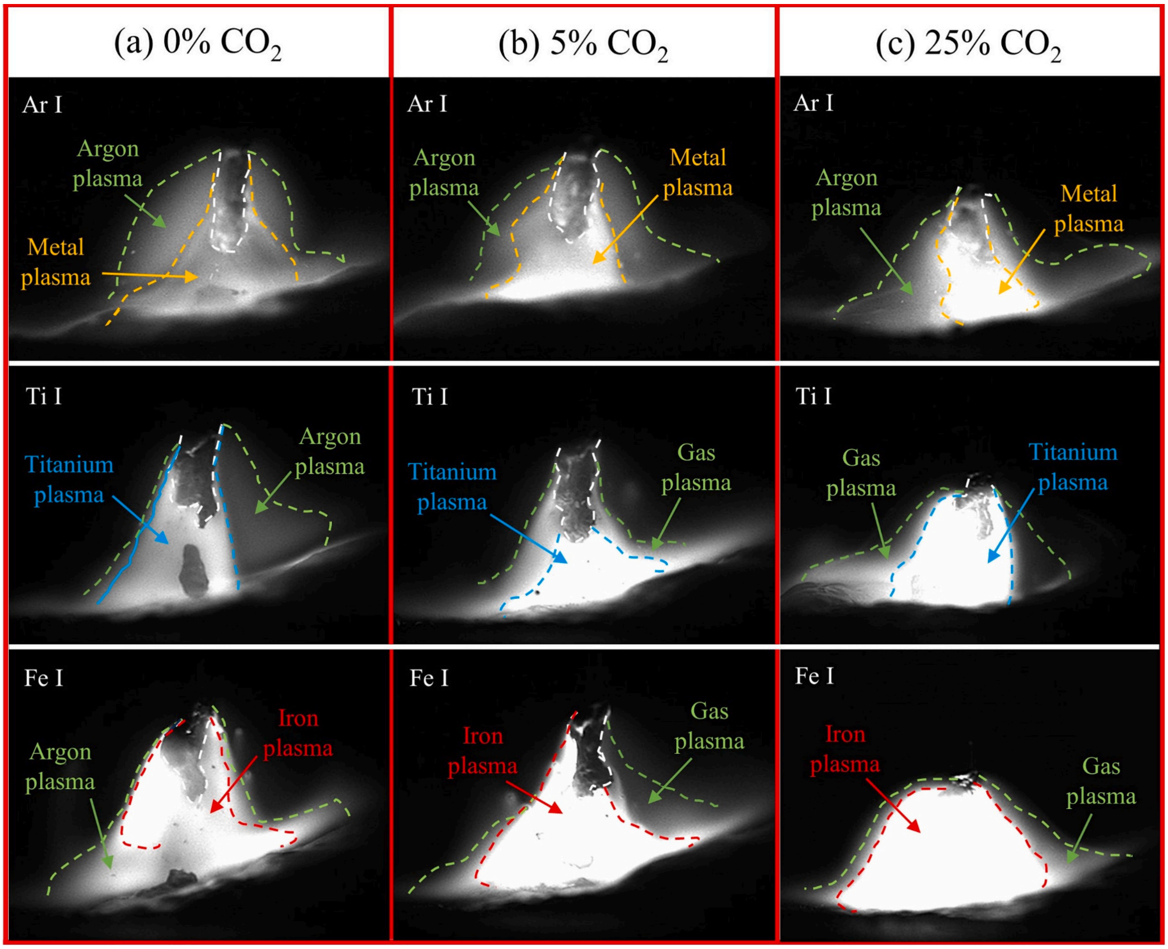

Fig. 15. Arc plasma distributions at 310 A at CO_2 concentrations of 0 % (a), 15 % (b), and 25 % (c) in the shielding gas.

Section 3.1, the unmelted flux column consistently remained at the wire tip across all conditions. Notably, the flux primarily comprises rutile TiO_2 covered by the metal sheath of the wire. Notably, the melting points of titanium and titanium dioxide are 1725 and 1843 °C, respectively, exceeding those of iron and iron oxide of 1538 and 1565 °C, respectively.

In GMAW, incorporating CO_2 into the shielding gas mixture alters the force dynamics governing the droplet transfer, which affects the interplay between electromagnetic forces, surface tension, and gas flow dynamics. Changing CO_2 concentration can affect surface tension and gas flow dynamics, but the electromagnetic force is typically the primary factor considered in modifying metal transfer behavior when adding CO_2 to the shielding gas. The presence of CO_2 alters the electrical conductivity and plasma properties of the arc, affecting the electromagnetic force acting on the molten metal droplet. This modification can influence droplet detachment frequency, size, and trajectory, ultimately impacting the overall metal transfer behavior during welding [24,25].

Within the context of FCAW, it can be inferred that the current predominantly follows the path within the metal sheath due to the low electrical conductivity of the flux. This results in Joule heating, and the thermal conduction from the arc heats the metal sheath. Conversely, the flux experiences heating from the molten metal sheath, flux, and arc through thermal conduction. Additionally, Ueno et al. reported the generation of an unmelted flux column at the wire tip due to the high specific heat and low thermal conductivity of rutile in the flux [26]. Consequently, the metal sheath exhibits a higher melting rate than the flux, causing the retention of a flux column at the wire tip during welding with the rutile flux-cored wire.

The presence of an unmelted flux is deemed to have a significant role in the metal transfer characteristics during welding with a cored wire. Trinh et al. noted that the unmelted flux column could hinder the effectiveness of the electromagnetic force in droplet separation, necessitating a higher transition current for spray transfer in welding with a metal-cored wire [21]. In this scenario, the unmelted flux exposed to the arc remains at the wire tip. The molten metal is required to descend and accumulate at the end of the flux column, as illustrated in Fig. 16(b). Droplet separation occurs when gravity and electromagnetic forces collaborate to form a neck on the droplet, as depicted in Fig. 16(c). The mechanism suggests that an elongated flux column prolongs the droplet generation to the detachment time.

Fig. 17 illustrates the distributions of titanium and iron plasmas. The images in **Fig. 17(a)** and **(b)** were retrieved from Fig. 14(b), at a welding current of 250 A with 15 % CO_2 in the shielding gas. The titanium vapor was concentrated beneath the flux column at the wire tip. The root of titanium vapor was attached at a lower position than the gas plasma position. On the other hand, the iron plasma was distributed from the overhead of the droplet, forming a bell-shaped plasma arc that extended to the weld pool. A schematic of the gas, titanium, and iron plasma is proposed in Fig. 17(c). Titanium was exclusively present within the wire's flux component. Titanium vapor emanated from the flux column area, diffusing into the arc and becoming concentrated beneath the end of the flux column. As a result, its evaporation was restricted from occurring at a higher position than the solid part of the wire sheath encompassing the flux column, as the sheath acted as a barrier. Conversely, iron, characterized by a lower boiling point than titanium (2861 °C compared to 3287 °C), evaporated at a higher position on the surface of the molten metal, originating from the metal sheath. Consequently, the iron plasma enveloped the titanium plasma and was

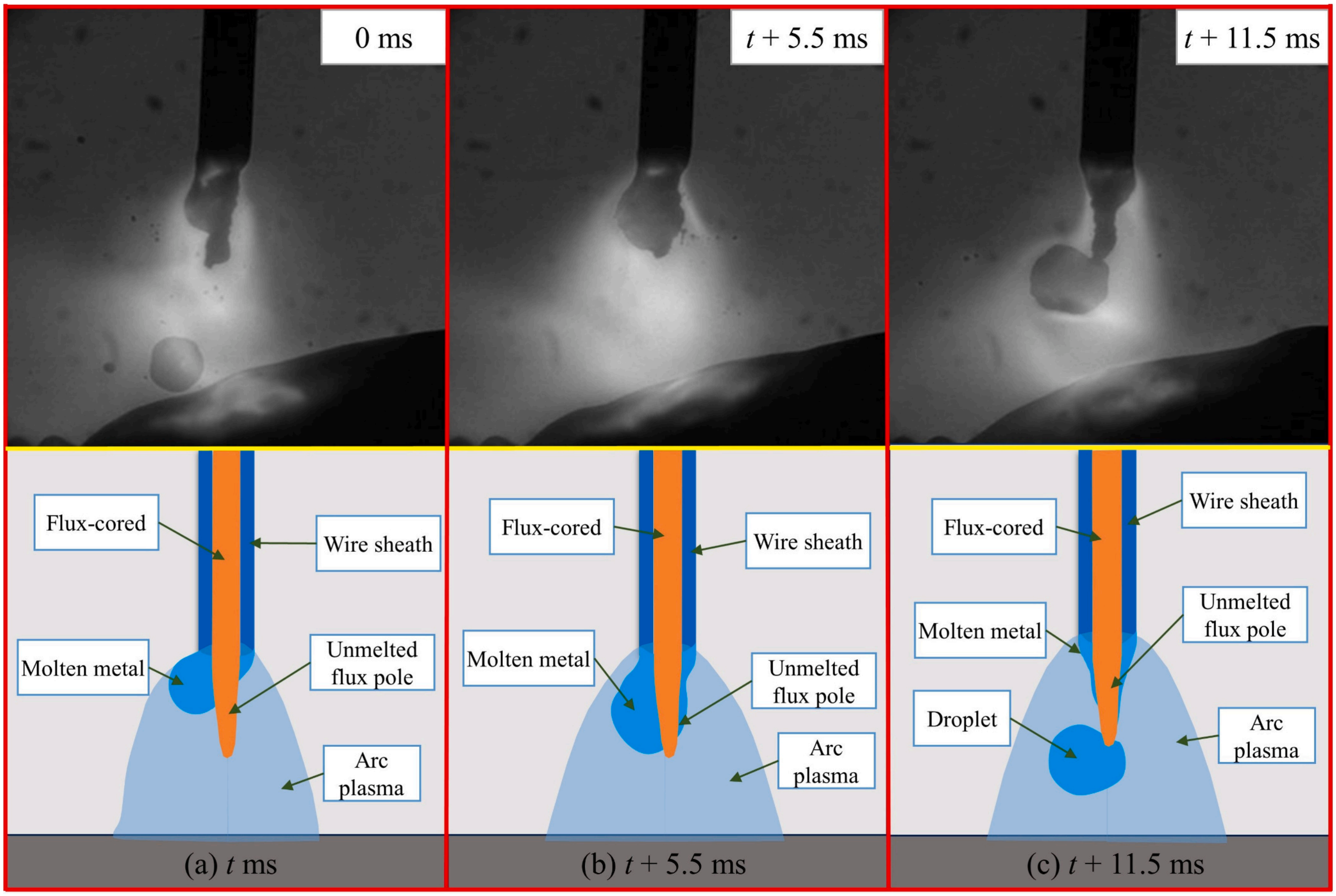

Fig. 16. Formation and detachment of a droplet at 190 A in pure argon gas.

covered by the gas plasma.

Fig. 18 presents a mechanism of the metal transfer behavior of the rutile flux-cored wire under the effect of the shielding gas, typically represented for welding at 250 A. As explained, the molten metal should accumulate at the end of the flux column sufficiently to detach from the wire tip. Thus, the length of the flux column contributed to the downward velocity of molten metal flows, as drawn in Fig. 18(a). At the same welding current, when the CO_2 concentration increased, the flux column was shortened owing to the arc constriction that focused the arc heating under the unmelted flux column. The broadened titanium plasma indicated higher flux evaporation due to this phenomenon, as observed in **Figs. 13, 14, and 15**. The gas and iron plasmas were moved down to attach under the droplet, as described in Fig. 18(b).

The addition of a moderate CO_2 concentration resulted in a slight increase in arc pressure. Nonetheless, it was hypothesized that the dominant factor influencing the metal transfer behavior was the shortening of the flux column. However, with a significantly high CO_2 concentration, the arc pressure under the droplet was deemed to prevail, impeding the detachment process. This phenomenon led to a reduction in metal transfer frequency at a CO_2 concentration of 25 %, as described in Fig. 18(c).

The metal transfer characteristics of FCAW in this study were thought to be influenced by the internal relationship between the exposed length of the flux column at the wire tip and the CO_2 concentration. A long flux column would raise the time from generation to detachment of a droplet. As mentioned above, the flux column was always observed due to a high melting of the wire sheath. The increase in CO_2 concentration caused a concentrated arc heating beneath the flux column, which contributed to a decrease in the flux length.

The duration of one cycle of droplet transfer was determined by the balance between the downward velocity of the molten metal to form a droplet and the flux length state. The molten metal velocity was thought to be impacted by the electromagnetic force, which was effective when the welding current increased. On the other hand, the shortening of the flux column was attributed not only to the increasing CO_2 concentration, as explained above, but also to the increasing welding current. The increased welding current contributed to a higher arc temperature, which increased the melting rate of the flux column to reduce its length. Consequently, the critical CO_2 concentration for a peak of metal transfer frequency was decreased when the welding current was increased, as observed in Fig. 2.

Notably, the peak frequencies at welding currents of 280 and 310 A remained consistent at 5 % CO_2. The metal sheath was heated by the Joule heating effect, which was reported to be more significant on the wire melting rate when the welding current increased, particularly above 280 A [27,28]. The effective Joule heating led to faster melting of the metal sheath, resulting in a relatively increased length of the flux column compared to the end of the metal sheath. As a result, the peak frequency was obtained at a consistent CO_2 concentration when the welding current exceeded 280 A up to 310 A.

Finally, effects of titanium vapor mixture into the plasma on metal transfer characteristics through the change in thermodynamic and transport properties of plasma are briefly discussed. As presented above, the flux is transferred to the weld pool together with the metal droplets in FCAW. However, because the temperature of the flux increases due to the heat input from the arc plasma, part of the flux evaporates and mixes with the arc. The elements in the flux have different ionization potentials and atomic weights from those of the shielding gas, so their mixing significantly changes the thermodynamic and transport properties of the arc plasma. This change also affects the temperature and velocity

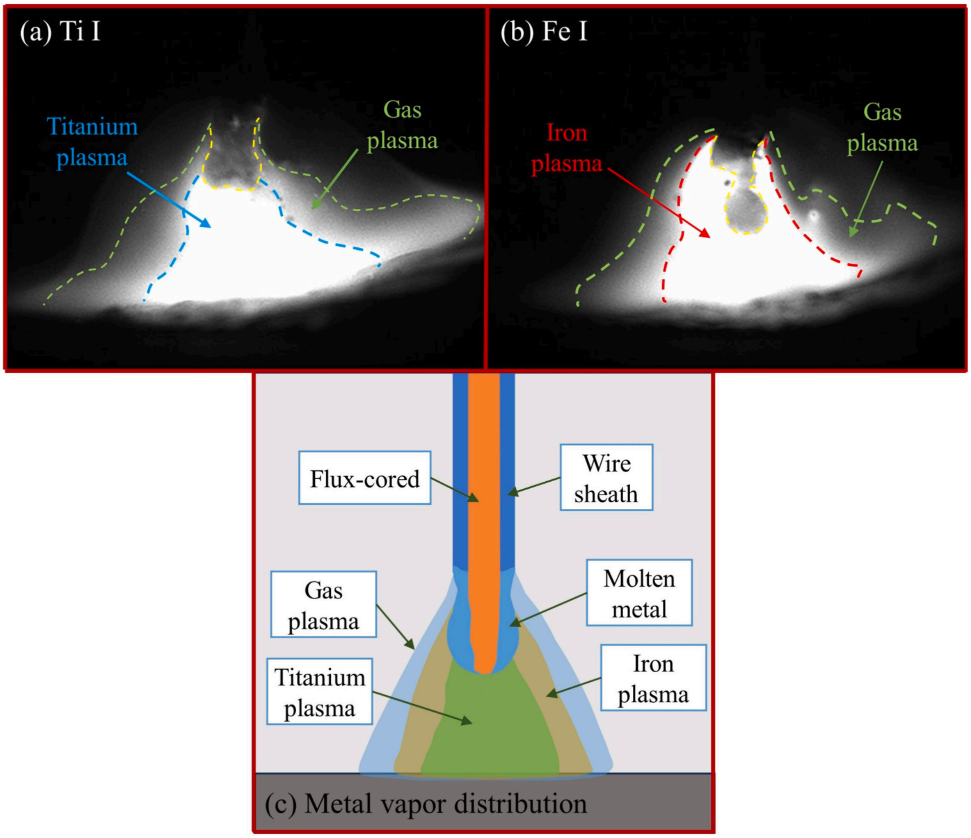

Fig. 17. Titanium plasma (a), iron plasma (b), and schematic of metal plasma distributions (c).

distributions of the arc as well as the current path in the arc. In particular, the current path is important because it governs the Lorentz force to be the main driving force for detaching the droplet, and the arc pressure below the droplet to suppress the droplet detachment.

As described in the introduction, there have been several papers reporting the effect of the sodium element contained in the metal flux on the arc and metal transfer in metal-cored arc welding.

Trinh et al. fabricated prototype wires with different sodium contents added to the metal flux and used them to experimentally observe the metal transfer behavior at a current of 220 A with Ar + 20 %CO_2 as the shielding gas [16]. They reported that iron vapor evaporated from the droplet bottom, while sodium vapor mainly evaporated from the molten wire tip or the neck between the wire and the droplet because of its low boiling point. Due to the low ionization potential of sodium atom, a new current path of sodium plasma was directly formed from the tip or neck of the molten wire through the arc plasma to the weld pool, bypassing the inside of the droplet. The formation of this new current path was considered to reduce the current of the iron plasma conducting from the droplet bottom reducing the arc pressure and further enhance the electromagnetic force acting on the neck to promote droplet detachment, thereby increasing the metal transfer frequency.

Bui et al. used the same prototype wires and conducted experiments using pure argon shielding gas and a high current of up to 310 A [17]. In GMAW using a solid wire, a large amount of iron vapor evaporated from the droplets is mixed into the arc. As a result, in the region near the arc axis under the droplet, the metal vapor concentration increases, and the arc temperature decreases due to radiation loss of the metal vapor, resulting in a decrease in electrical conductivity. Consequently, the current avoids the metal vapor plasma and conducts primarily through the surrounding shielding gas plasma. This reduces the arc pressure directly below the droplet, and the Lorentz force is more easily applied to the neck portion at the top of the droplet, making it easier for the droplet to transfer in a spray transfer mode. On the other hand, in GMAW using a metal-cored wire with a metal flux containing a large amount of sodium element, sodium vapor is mixed into the metal vapor plasma. The mixture is considered to raise the electrical conductivity of the metal vapor plasma around the arc axis, increasing the proportion of current conducting through the metal vapor plasma. This current increases the arc pressure directly below the droplet. As a result, it was found that even in the high current range where a streaming transfer mode was seen in a solid wire case, a project transfer mode appeared in metal-cored wire case.

Also in FCAW, elements contained in the flux evaporate and mix with the plasma, which is thought to induce an effect similar to that in the metal-cored wire case. In rutile FCAW, the main component of the flux is TiO_2. We briefly discuss the effects of this main component, when it evaporates and is mixed into the metal vapor plasma, on the thermodynamic and transport properties of plasma, and further on the current path and the Lorentz force. The ionization potential strongly influences the electrical conductivity of the plasma. The ionization potentials of iron, titanium, and sodium are 7.9, 6.8, and 5.1 eV, respectively. Therefore, the electrical conductivity of titanium plasma is predicted to be higher than that of iron plasma and lower than that of sodium plasma. The atomic weight affects the thermal conductivity, viscosity, etc. of the plasma. The atomic weights of iron, titanium, and sodium are 55.8, 47.9 and 23.0, respectively. The atomic weight of titanium is slightly lower than that of iron and much larger than that of sodium. Therefore, the mass density, thermal conductivity, viscosity of titanium plasma are expected to be similar levels with those of iron plasma. As shown in Figs. 13, 14, and 15, the titanium element in the metal vapor plasma is distributed in large amounts in the region near the arc axis around the flux. From this, it is thought that the mixture of titanium vapor into the metal vapor plasma increases the electrical conductivity of this region, and the proportion of current conducting through the metal vapor

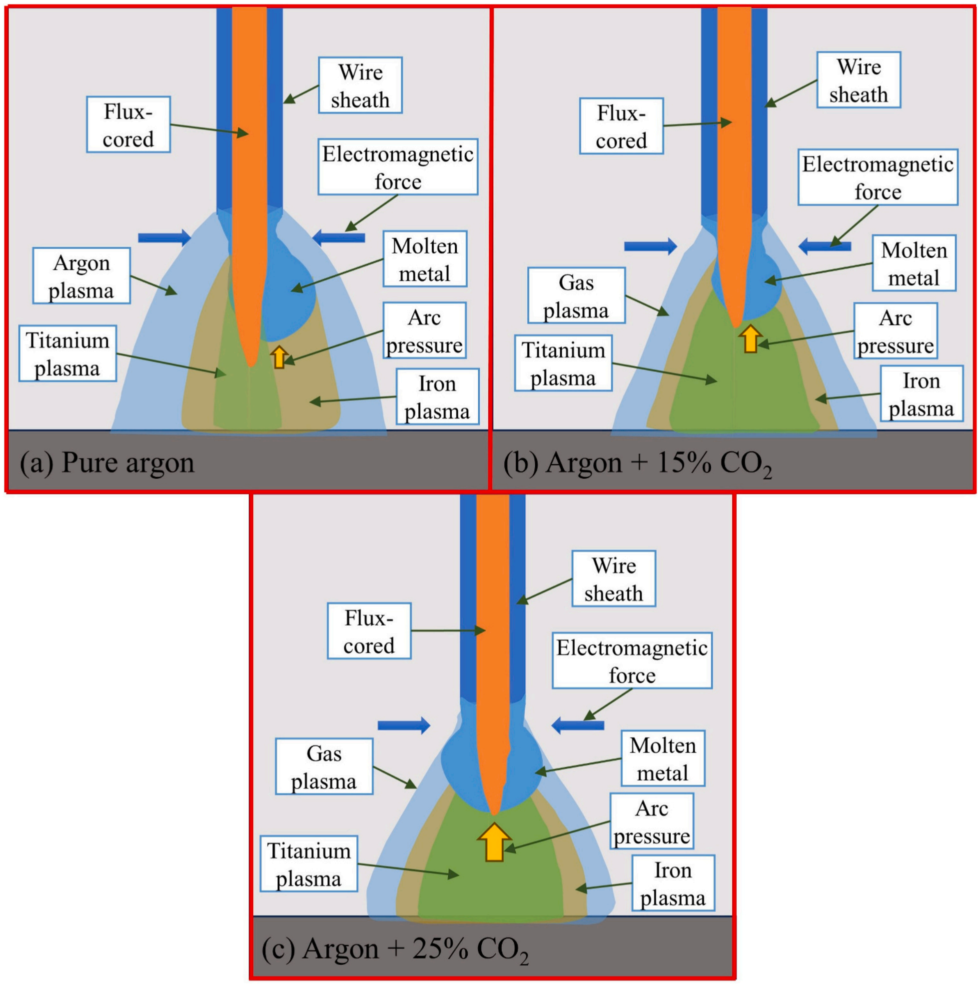

Fig. 18. Mechanism of the metal transfer behavior of the rutile flux-cored wire under the effect of the shielding gas.

plasma increases. It might increase the arc pressure at the bottom of the droplet, suppressing the detachment of the droplet. However, compared with the case of sodium vapor mixture reported by Bui et al. [17], the effect is thought to be smaller due to the difference in ionization potential.

In this study, the experiments were conducted using only one type of FCAW wire. In order to discuss the influence of each element contained in the flux, it is essential to carry out a parametric study using prototype wires with different flux compositions. For clarifying the effect of the TiO_2 content in the flux on the metal transfer characteristics, prototype wires are currently prepared. That result will be reported in future.

4. Conclusion

We conducted a parametric investigation of the CO_2 concentration in an Ar–CO_2 shielding gas mixture to optimize the metal transfer process in FCAW with a rutile flux-cored wire. Observation approaches were employed to measure the metal transfer frequency, and spectral band-pass filters were utilized to analyze arc characteristics. The conclusions can be summarized as follows.

1. The droplet transfer increased when a small portion of CO_2 was included and decreased when the CO_2 concentration increased. The transfer frequency achieved a peak of 105.7, 154.8, 208.0, 270.3, and 304.0 Hz at a welding current of 190, 220, 250, 280, and 310 A with a critical CO_2 concentration of 20 %, 15 %, 15 %, 5 %, and 5 %, respectively.
2. A molten droplet was generated at the end of the metal sheath and beside an unmelted flux column. The molten droplet must flow downward and accumulate at the end of the flux column to separate for a detachment.
3. Titanium vapor was evaporated at the end of the flux column, where an area of the flux column was exposed to the arc. Meanwhile, the iron vapor could be evaporated at a higher position at the end of the metal sheath.
4. The length of the flux column directly impacts the duration of one droplet transfer cycle. The increased carbon dioxide concentration leads to a constricted arc plasma, causing flux column melting and shortening, temporarily resulting in an increased metal transfer frequency. However, the frequency decreased when a high CO_2 concentration was present, leading to a significantly increased arc pressure.
5. As the welding current increased, the flux column shortened due to the increased arc temperature, which shifted the maximum transfer frequency to a lower CO_2 concentration.

CRediT authorship contribution statement

Ngoc Quang Trinh: Visualization, Investigation, Writing – original draft. **Khoi Dang Le:** Visualization, Investigation, Writing – original draft. **Shinichi Tashiro:** Conceptualization, Writing – review & editing. **Tetsuo Suga:** Project administration. **Shuji Sasakura:** Validation, Resources. **Kazuhiro Fukuda:** Validation, Resources. **Anthony B. Murphy:** Validation. **Hanh Van Bui:** Validation. **Manabu Tanaka:**

Validation, Supervision.

Funding

This research is funded by Hanoi University of Science and Technology (HUST) under project number T2023-TĐ-020.

This research was also supported by JSPS KAKENHI (Grant Number JP21K04710).

Declaration of competing interest

The authors declare that they have no known competing financial interests or personal relationships that could have appeared to influence the work reported in this paper.

Acknowledgements

This work was supported by the Project on Design & Engineering by Joint Inverse Innovation for Materials Architecture (DEJI2MA) from the Ministry of Education, Culture, Sports, Science and Technology (MEXT), and an OU Master Plan Implementation Project promoted under Osaka University.

The authors are grateful for supporting this study through a joint research agreement between the School of Mechanical Engineering, Hanoi University of Science and Technology, Vietnam; Joining and Welding Research Institute, Osaka University, Japan; Kobe Steel Ltd., Japan; and Thai Kobelco Welding Co., Ltd., Thailand.

References

[1] Brien AO. Welding Handbook 1987;2. https://doi.org/10.1007/978-1-349-10624-0.
[2] Zhang Y, Jia C, Zhao B, Hu J, Wu C. Heat input and metal transfer influences on the weld geometry and microstructure during underwater wet FCAW. J Mater Process Technol 2016;238:373–82. https://doi.org/10.1016/j.jmatprotec.2016.07.024.
[3] Ma Q, Luo C, Liu S, Li H, Wang P, Liu D, et al. Investigation of arc stability, microstructure evolution and corrosion resistance in underwater wet FCAW of duplex stainless steel. J Mater Res Technol 2021;15:5482–95. https://doi.org/10.1016/j.jmrt.2021.11.023.
[4] Baumé E, Bonnet C, Liu S. Assessing metal transfer stability and spatter severity in flux cored arc welding. Sci Technol Weld Join 2001;6:139–48. https://doi.org/10.1179/136217101101538677.
[5] Kah P, Latifi H, Suoranta R, Martikainen J, Pirinen M. Usability of arc types in industrial welding. Int J Mech Mater Eng 2014;9:1–12. https://doi.org/10.1186/s40712-014-0015-6.
[6] Bang KS, Jung HC, Han IW. Comparison of the effects of fluorides in rutile-type flux cored wire. Met Mater Int 2010;16:489–94. https://doi.org/10.1007/s12540-010-0622-6.
[7] Wang Y, Zhang YQ, Wang B, Wang ZJ. Study on metal transfer and welding spatter characteristics of basic flux cored wire. Appl Mech Mater 2014;477–478:1369–72. https://doi.org/10.4028/www.scientific.net/AMM.477-478.1369.
[8] Palani PK, Murugan N. Prediction of delta ferrite content and effect of welding process parameters in claddings by FCAW. Mater Manuf Process 2006;21:431–8. https://doi.org/10.1080/10426910500471409.
[9] Senthilkumar B, Kannan T. Effect of flux cored arc welding process parameters on bead geometry in super duplex stainless steel claddings. Measurement (Lond) 2015;62:127–36. https://doi.org/10.1016/j.measurement.2014.11.007.
[10] Lancaster JF. The physics of fusion welding part 2: mass transfer and heat flow. IEE Proceedings B: Electric Power Applications 1987;134:297–316. https://doi.org/10.1049/ip-b.1987.0047.
[11] Matsuda F;, Ushio M;, Tsuji T;, Mizuta T. Arc Characteristics and Metal Transfer with Flux-Cored Electrode in CO_2 Shielding (Report I) : Effect of Geometrical Shape in Wire Cross-section on Metal Transfer in Stainless Steel Wire. 1979.
[12] Yamamoto E, Yamazaki K, Suzuki K, Koshiishi F. Effect of flux ratio in flux-cored wire on wire melting behavior and fume emission rate. R154. Welding in the World 2010:54.
[13] Trinh NQ, Tashiro S, Suga T, Kakizaki T, Yamazaki K, Morimoto T, et al. Effect of flux ratio on droplet transfer behavior in metal-cored arc welding. Metals (Basel) 2022:12. https://doi.org/10.3390/met12071069.
[14] Starling CMD, Modenesi PJ. Metal transfer evaluation of tubular wires. Weld Int 2007;21:412–20. https://doi.org/10.1080/09507110701510832.
[15] Valensi F, Pellerin N, Pellerin S, Castillon Q, Dzierzega K, Briand F, et al. Influence of wire initial composition on anode microstructure and on metal transfer mode in GMAW: noteworthy role of alkali elements. Plasma Chem Plasma Process 2018;38:177–205. https://doi.org/10.1007/s11090-017-9860-4.
[16] Trinh NQ, Tashiro S, Tanaka K, Suga T, Kakizaki T, Yamazaki K, et al. Effects of alkaline elements on the metal transfer behavior in metal cored arc welding. J Manuf Process 2021;68:1448–57. https://doi.org/10.1016/j.jmapro.2021.06.061.
[17] Van Bui H, Trinh NQ, Tashiro S, Suga T, Kakizaki T, Yamazaki K, et al. Individual effects of alkali element and wire structure on metal transfer process in argon metal-cored arc welding. Materials 2023;16. https://doi.org/10.3390/ma16083053.
[18] Ushio M, Ikeuchi K, Tanaka M, Seto T. Effects of shielding gas on metal transfer. Weld Int 1995;9:462–6. https://doi.org/10.1080/09507119509548831.
[19] Liao MT, Chen WJ. A Comparison of Gas Metal Arc Welding with Flux-Cored Wires and Solid Wires Using Shielding Gas 1999;15.
[20] Wang W, Liuandj SE. Flux Cored Arc Welding: Arc Signals, Processing and Metal Transfer Characterization Certain arc voltage signals are verified as indicators of transfer modes and thereby arc stability. n.d.
[21] Trinh NQ, Tashiro S, Suga T, Kakizaki T, Yamazaki K, Lersvanichkool A, et al. Metal transfer behavior of metal-cored arc welding in pure argon shielding gas. Metals (Basel) 2022:12. https://doi.org/10.3390/met12101577.
[22] Świerczyńska A, Varbai B, Pandey C, Fydrych D. Exploring the trends in flux-cored arc welding: scientometric analysis approach. Int J Adv Manuf Technol 2023. https://doi.org/10.1007/s00170-023-12682-6.
[23] Haidar J, Lowke JJ. Effect of CO2 shielding gas on metal droplet formation in arc welding. IEEE Transactions on Plasma Science 1997;25:931–6. https://doi.org/10.1109/27.649598.
[24] Ogino Y, Hirata Y, Murphy AB. Numerical simulation of GMAW process using Ar and an Ar–CO2 gas mixture. Welding in the World 2016;60:345–53. https://doi.org/10.1007/s40194-015-0287-3.
[25] Wang LL, Lu FG, Wang HP, Murphy AB, Tang XH. Effects of shielding gas composition on arc profile and molten pool dynamics in gas metal arc welding of steels. J Phys D Appl Phys 2014:47. https://doi.org/10.1088/0022-3727/47/46/465202.
[26] Ueno R, Komen H, Shigeta M, Tanaka M. Numerical simulation of droplet transfer with TiO2 flux column during flux cored arc welding by 3D smoothed particle hydrodynamics method. Quarterly Journal Of The Japan Welding Society 2020;38:84–8.
[27] Shimizu H, Yokota Y, Itoh T, Kurokawa T, Ushio M. Joule heating of solid wires in MAG welding. Weld Int 2005;19:761–72. https://doi.org/10.1533/wint.2005.3488.
[28] Modenesi PJ, Starling CMD, Reis RI. Wire melting phenomena in gas metal arc welding. Sci Technol Weld Join 2005;10:610–6. https://doi.org/10.1179/174329305X57446.